Asian Journal of Chemistry; Vol. 37, No. 9 (2025), 2176-2182
ASIAN JOURNAL OF CHEMISTRY
https://doi.org/10.14233/ajchem.2025.34137

Biosynthesis of ZnO Nanoparticles using Marine Plant *Syringodium isoetifolium*: Unveiling Antioxidant, Antibiofilm and Anticancer Potentials

S.K. HANSIKA, G. DHANRAJ and R.R. SUBBURAYAN*,

Department of Prosthodontics, Saveetha Dental College and Hospitals, Saveetha Institute of Medical and Technical Sciences, Saveetha University, Chennai-600077, India

*Corresponding author: E-mail: surabio01@yahoo.com

Received: 27 May 2025 *Accepted*: 23 July 2025 *Published online*: 30 August 2025 AJC-22097

The present study focuses on the green synthesis of zinc oxide (ZnO) nanoparticles using an aqueous extract of the seagrass *Syringodium isoetifolium*, along with their physico-chemical characterization and assessment of antioxidant, antibiofilm, and cytotoxic properties. Preliminary characterization of the *S. isoetifolium*-mediated zinc oxide nanoparticles (SI-ZnO NPs) using UV-Vis spectroscopy showed maximum absorption at 374 nm. FTIR and XRD spectroscopy analysis evidenced the promising functional groups and crystalline structure associated with ZnO nanoparticles. The SEM images showed irregularly shaped cubic crystals with grain size of 67.24 nm. Antioxidant assay results affirmed that SI-ZnO NPs strongly neutralized DPPH radicals in a dose-dependent manner (22% to 74%). Biofilm inhibitory activity revealed that SI-ZnO NPs prodigiously impaired (12 to 84%) biofilm formation by the oral pathogen *Candida albicans*. Confocal laser scanning microscopic visuals emphasized that SI-ZnO NPs reduced viability and distorted the *C. albicans* biofilm architecture. Artemia cytotoxicity assays revealed that SI-ZnO NPs exhibited an LC_{50} value of 62.48 µg/mL, while the hemolytic analysis confirmed their biosafety profile. The significant biomedical properties and biocompatibility of SI-ZnO NPs will pave the way for their effective utilization in pharmacology and healthcare settings.

Keywords: *Syringodium isoetifolium*, ZnO nanoparticles, Antioxidant activity, Antibiofilm inhibitory activity, Cytotoxicity.

INTRODUCTION

Nanotechnology enables precise control of materials at the atomic and molecular levels, enhancing properties like conductivity, wettability and light interaction [1,2]. These improved properties yield superior functionality compared to their larger-scale counterparts. Conventional physical and chemical approaches for nanoparticle synthesis present several limitations. Chemical methods typically involve hazardous reagents and organic solvents, raising concerns about environmental contamination and potential risks to human health. Similarly, physical techniques require substantial energy input and elevated temperatures, contributing to environmental stress. However, nanoparticles synthesized through these routes often exhibit poor biocompatibility, thereby restricting their applicability in biomedical fields [3,4]. Considering the negative impacts of conventional methods, green nanoparticle synthesis has emerged as a promising alternative, wherein biological materials such as extracts/supernatants from plants, bacteria, fungi and agricultural wastes were used to synthesize nanoparticles [6]. Biogenic nanoparticles offer significant advantages by eliminating the need for toxic chemicals and high energy inputs. They are sustainable, eco-friendly, biocompatible and well-suited for therapeutic applications [6].

Oral diseases are among the most prevalent diseases globally, exerting significant health and economic challenges that drastically impair the quality of life for affected individuals. The most widespread oral health issues worldwide are dental caries, periodontal disease, tooth loss and lip cancers [7]. Dental caries, also referred to as cavities or tooth decay, can result in severe discomfort and eventual tooth loss if not addressed. The consequences of this disease extend beyond the faciomaxillary region, impacting an individual's general health [8]. In general, oral cavities provide a conducive environment for the entry of both bacterial (*Streptococcus* spp., *Porphyromonas* spp., *Propionibacterium* spp. and *Velionella* spp.) and fungal (*Candida* spp.) pathogens that are involved

in caries formation [9,10]. Amongst these, *Candida albicans* is a notable fungal pathogen known for its virulence and ability to form biofilms. It enters through oral mucosa and adheres to biotic and abiotic surfaces, such as dental prostheses. The complex 3D biofilm structure of *C. albicans* protects it from antifungal agents, making it more challenging to treat. This further exacerbates systemic diseases and results in nosocomial infections. Currently, the antibiotics and synthetic antioxidants used to mitigate candidal infections and reactive oxygen species (ROS) were found to cause severe side effects such as allergic reactions, gastrointestinal issues, hormonal defects and interference with medications [11,12]. In this context, developing nanoantibiotics (nAbts) utilizing engineered nanoparticles presents a viable and sustainable way to address drug resistance [13]. Their smaller size enhances bacterial interaction, circumvents cellular barriers and improves drug delivery and treatment efficacy at lower doses [14]. Similarly, metal oxide-based nanoantioxidants were found to reduce oxidative stress-related diseases.

Considering green nanoparticle synthesis, plants are often preferred rather than microbes due to their rich phytoconstituents, such as polyphenols, flavonoids, alkaloids, *etc.* which serve as reducing and stabilizing agents during nanoparticle formation [15,16]. Besides the terrestrial medicinal plants, marine plants such as seagrass, seaweeds and mangroves were considered untapped reservoirs and promising candidates for the green fabrication of metallic nanoparticles [17,18]. Marine seagrass is one of the most promising flowering plants in shallow ocean regions. These underwater meadows play a crucial role in the coastal ecosystem; they provide a habitat for diverse aquatic organisms and improve water quality by stabilizing the sediments [19]. In particular, the nanoparticles synthesized through biological routes are being developed as antimicrobial agents in wound healing, as targeted drug delivery systems for cancer treatment, improving tissue regeneration, diagnostic imaging and *in vivo* models substantiated appreciable control in blood glucose level and lipid profile [16]. Recently, researchers explored the biological activities of nanoparticles derived from various seagrass species as these species are the rich sources of nutrients and bioactive compounds. Recently, Ameen *et al*. [20] highlighted bioactive compounds isolated from seagrass species exhibited striking antibacterial activity against MRSA, anti-HIV activity, antioxidant, antiviral, skin-regenerating, antilarval and antifeedant activities. Furthermore, Ahila *et al.* [21] evidenced that polysaccharides and proteins extracted from seagrass *Syringodium iosetifolium*-mediated silver NPs had superior antibacterial properties. Thinh *et al.* [22] studied the formation of NPs using pectin from *Enhalus acoroides*. More recently, Narayanan *et al.* [23] and Sundar *et al.* [24] demonstrated the promising antibacterial, antibiofilm, antioxidant, cytotoxic and dye-degradative properties of TiO_2 NPs produced using *S. iosetifolium* and *Cymodocea serrulata*.

Although many studies explored the silver and titanium metal-based nanoparticles from seagrass, only a countable number of reports are available on ZnO NPs from seagrass. Viewing the biomedical properties of nanoparticles derived from seagrass, this study explores the fabrication of ZnO nanoparticles using seagrass *Syringodium isoetifolium.* Further, it highlights its promising antioxidant, biofilm inhibitory, cytotoxic and hemolytic properties.

EXPERIMENTAL

All chemicals used were of analytical grade and used without further purification. Zinc acetate dihydrate ($Zn(CH_3COO)_2{\cdot}2H_2O$) was used as zinc precursor (Loba Chemie, India) and deionized water were used throughout the process.

UV-Vis spectrophotometry was used to measure the optical absorbance of SI-ZnO NPs, covering a range from 200 to 800 nm. The biomolecules associated with the SI-ZnO NPs were identified with FTIR spectrophotometer (Perkin-Elmer Spectrum 400) within the spectral range of 4000-700 cm^{-1}. The crystalline structure of SI-ZnO NPs was analyzed by X-ray diffraction (XRD) over a 2θ range of 20º-80º. For scanning electron microscopy (SEM), the nanoparticle powder was mounted on carbon tape, gold-coated and examined under high vacuum in secondary electron mode at an accelerating voltage of up to 30 kV. Elemental composition was assessed using energy-dispersive X-ray spectroscopy (EDX).

Synthesis of ZnO nanoparticles: For this study, seagrass *Syringodium isoetifolium* was harvested from the coastal area of Kanyakumari (8.0847º N, 77.5486º E), India. After collection, the plant was cleaned to eliminate any attached organisms, air-dried and ground into a fine powder. Then, 5 g of *S. isoetifolium* powder was boiled in 100 mL of Milli Q water at 60 ºC for 30 min and filtered using Whatman No. 1 filter paper. A 0.01 M solution of $Zn(CH_3COO)_2{\cdot}2H_2O$ was then mixed with 50 mL of *S. isoetifolium* extract and kept in a water bath for 3 to 5 h at 70 ºC, with continuous stirring. The resulting light white sediment was separated by spinning at 4000 rpm for 10 min and dried at 100 ºC overnight. Finally, the dried material was calcined (400-450 ºC) for 4 h to obtain SI-ZnO NPs in powder form.

Antioxidant evaluation: A DPPH assay was performed to determine the antioxidant potential of SI-ZnO NPs. For this, varying the concentrations of (25 to 100 μg/mL) of *S. isoetifolium* extract-mediated ZnO nanoparticles were mixed with 1 mL of 0.1 mM DPPH dissolved in methanol and 450 μL of 50 mM Tris-HCl buffer (pH 7.4) and then incubated for 30 min. The decrease in DPPH free radicals was measured based on the absorbance at 517 nm. Ascorbic acid was used as a reference [25] and the inhibition percentage was calculated.

Biofilm inhibition assay: In brief, 100 μL of overnight cultured *C. albicans* (MTCC183) was collected and adjusted to McFarland standard (1×10^8 cell/mL) using yeast malt broth and seeded in 96-multiwell plates. Then, different concentrations of SI-ZnO NPs (10 to 320 μg/mL) were added and incubated for 24 h at 37 ºC. After incubation, the biofilm inhibition (%) was determined by crystal violet using an ELISA reader [26].

Antibiofilm study: In the antibiofilm assay, *C. albicans* was allowed to form a biofilm on sterilized glass slides. These slides were then exposed to different concentrations of SI-ZnO NPs (160 and 320 μg/mL) and incubated at 37 ºC for

24 h. A control slide without the SI-ZnO NPs was also prepared. After the specified time interval, the slides were washed and stained with 0.1% acridine orange for examination under a Confocal Laser Scanning Microscope (CLSM) [26].

***Artemia* cytotoxicity:** The cytotoxicity of SI-ZnO NPs was determined using *Artemia salina* nauplii as a model organism. Briefly, varying concentrations (50 to 200 µg/mL) of SI-ZnO NPs were prepared in filtered seawater and transferred individually into a 24-multiwell plate. Subsequently, 10 *A. salina* (IVth instar stage) nauplii were introduced into each well-containing SI-ZnO NPs. A control well was maintained with seawater lacking SI-ZnO NPs and incubated for 24 h at 27 ºC. After the experimental duration, the number of live (%) and dead (%) nauplii was visually counted based on the movement and LC_{50} was calculated [21].

Hemolytic activity: The biocompatibility of the SI-ZnO NPs was determined by assessing its hemolytic property. In short, the blood samples were collected from volunteers and its coagulating activity was inhibited using 2.7% EDTA. The erythrocytes were prepared as a suspension by following Prakash *et al.* [25] method. About 0.1 mL of erythrocyte suspension was transferred to 96 multi-well plates, followed by varying concentrations (50 to 200 µg/mL) of SI-ZnO NPs and incubated for 1 h at 37 ºC. The entire content was centrifuged at 2000 rpm for 10 min. Thereafter, OD was read at 540 nm and the hemolysis (%) was calculated.

Statistical analysis: The results were subjected to mean ± SD and subsequently to One-Way ANOVA and further *post hoc* multiple comparisons using the SNK and Dunnett test with significant levels ($p < 0.05$).

RESULTS AND DISCUSSION

UV-visible studies: The production of ZnO NPs by *S. isoetifolium* was preliminarily confirmed through UV spectroscopy, with a unique absorption peak at 374 nm, attributed to the formation of surface plasmon resonance (SPR) (Fig. 1). This observation closely aligns with previous reports utilizing *Spirogyra hyalina* [27] and *Cymodocea serrulata* [28] extracts for the formation of ZnO NPs. The UV-Vis absorption peaks observed between 300–400 nm are the characteristic of ZnO nanoparticles indicating a narrow particle size distribution and confirming their nanoscale dimensions [29].

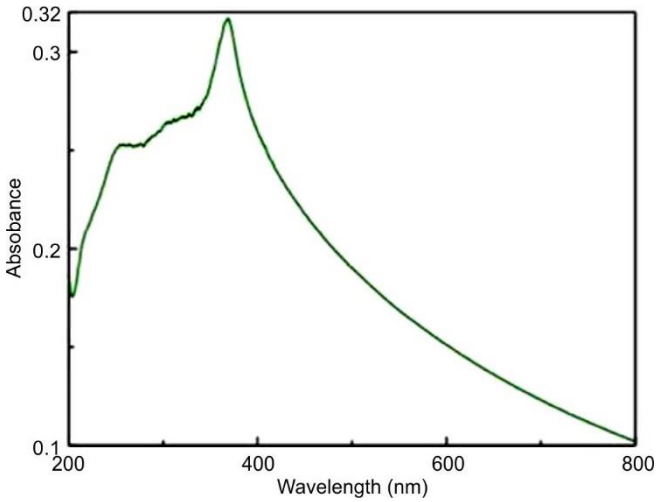

Fig. 1. UV-Vis of SI-ZnO NPs biosynthesized by *S. isoetifolium*

FTIR studies: FTIR was utilized to analyze the bioactive compounds attached to the nanoparticles surface (Fig. 2). This analysis explores the types of functional groups within the extract of *S. isoetifolium*, which are involved in the stabilization of ZnO NPs. The spectral analysis revealed that the functional groups associated with nanoparticles were observed at 3782.62 and 3638.27 cm^{-1} indicated hydroxyl groups (O–H) involved in hydrogen bonding. A peak at 2349.19 cm^{-1} suggested the presence of an alkyne group characterized by a C≡O stretching. The peak at 1410 cm^{-1} indicated the stretching of the sulfate (S=O) group, whereas a small peak at 871.11 cm^{-1} suggested the aromatic bending of the C-H group. Finally, the peak observed at 577 cm^{-1} confirmed the presence of ZnO nanoparticles, corresponding to the Zn–O stretching vibration and indicating the incorporation of ZnO. These groups formed the layered structures on the surface of nanoparticles, playing a crucial role in stabilizing these nanoparticles. Similar types of functional groups associated with ZnO NPs were reported from *Chrysopogon zizganioides* [30].

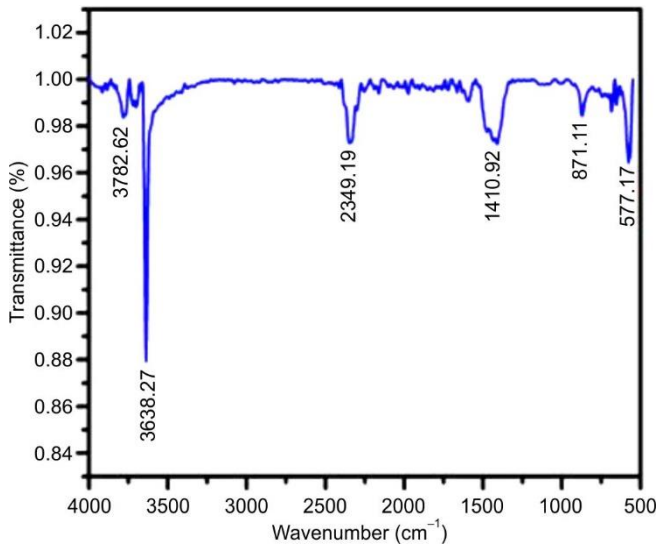

Fig. 2. FT-IR of SI-ZnO NPs biosynthesized by *S. isoetifolium*

XRD studies: The X-ray diffraction (XRD) pattern (Fig. 3) inferred that SI-ZnO NPs exhibited peaks at 34.23º, 35.12º, 38.35º, 48.72º, 56.23º, 64.51º and 69.11º correspond to the crystallographic planes (*hkl*) of ZnO NPs as per the reference data from the JCPDS file No. 079-2205. Specifically, the peaks are associated with the following crystallographic planes: (010), (002), (011), (012), (110), (013) and (020). The average grain size of SI-ZnO NPs was found to be 67.24 nm. In conformity with the present study, plants such as *A. indica*, *H. rosasinensis*, *M. koenig*, *M. oleifera* and *T. indica* also demonstrated high crystallinity same type of diffraction angles [31]. Similar results were observed by the ZnO nanoparticles from green algae *Spirogyra hyaline* extract [27]. This indicates that SI mediated ZnO NPs synthesis yielded a phase-pure product free from the additional phase impurities. Further, the sharp and well-defined peaks substantiated the crystalline nature of the synthesized ZnO nanoparticles.

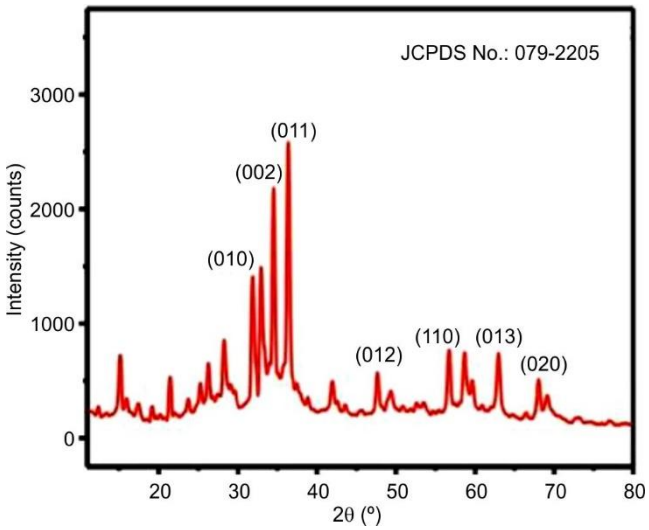

Fig. 3. XRD of SI-ZnO NPs biosynthesized by *S. isoetifolium*

Morphological studies: The ZnO nanoparticles derived from seagrass *S. isoetifolium* subjected to SEM study inferred that particles appeared as granular, irregularly shaped cubic crystals with rough surfaces (Fig. 4a). The elemental composition of the nanoparticles was analyzed using EDX analysis. The EDX spectrum (Fig. 4b), particularly within the energy range of 0.96 to 9.5 keV, displayed characteristic peaks corresponding to zinc, confirming the presence of ZnO nanoparticles.. In the EDX spectrum, Zn (40.5%) and O (30.8%) were predominantly detected. Subsequently, other elements such as carbon (19.7%) and calcium (9%) were recorded, likely originating from the seagrass *S. isoetifolium*. The morphological characteristics observed in the present study are in agreement with those reported for zinc oxide nanoparticles synthesized using *Cymodocea serrulata*, which exhibited irregular, cubic and rough-surfaced crystalline structures [30]. Similarly, green synthesis approaches employing *Atalantia monophylla* and *Costus igneus* leaf extracts have yielded ZnO nanoparticles with average crystalline sizes of approximately 30 nm [32,33].

Antioxidant activity: The antioxidant activity of the SI-ZnO NPs was evaluated using the DPPH method. The assay was performed by varying the concentrations (25-100 µg/mL) to gauge the green-synthesized ZnO NPs effectiveness in mitigating oxidative damage. At the lowest concentration (25 µg/mL), the SI-ZnO NPs showed 23.5% radical scavenging activity, slightly lower than the standard ascorbic acid (27.5%). However, at a higher concentration (100 µg/mL), the SI-ZnO NPs achieved 64.6% and ascorbic acid with 76.7%, respectively. The enhanced radical scavenging property of the SI-ZnO NPs in trapping radicals could be due to phytoconstituents within specific extracts (Fig. 5). This signifies that biosynthesized SI-ZnO NPs efficiently neutralized the free radicals, implying their ability to alleviate oxidative stress and thus suggesting that it could be a significant alternative to chemical antioxidants and further emphasizing the potential of the ZnO NPs in safeguarding biological systems from cellular oxidation.

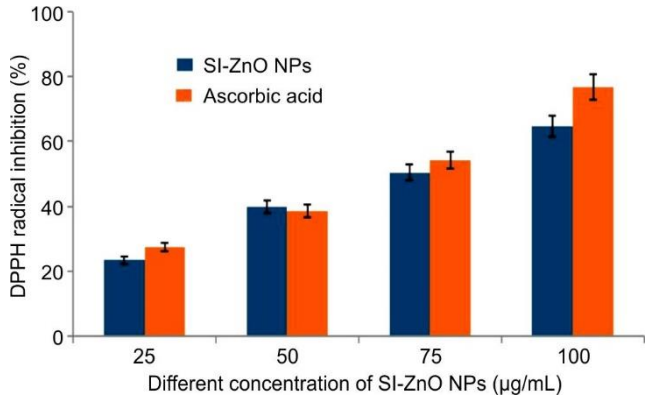

Fig. 5. DPPH radical scavenging activity of ascorbic acid and SI-ZnO NPs biosynthesized by *S. isoetifolium*

Biofilm inhibition: *C. albicans* is typically a part of the normal microbiota, existing harmlessly in various human body parts, such as the gastrointestinal tract, reproductive system, oral cavity and skin, without causing symptoms.

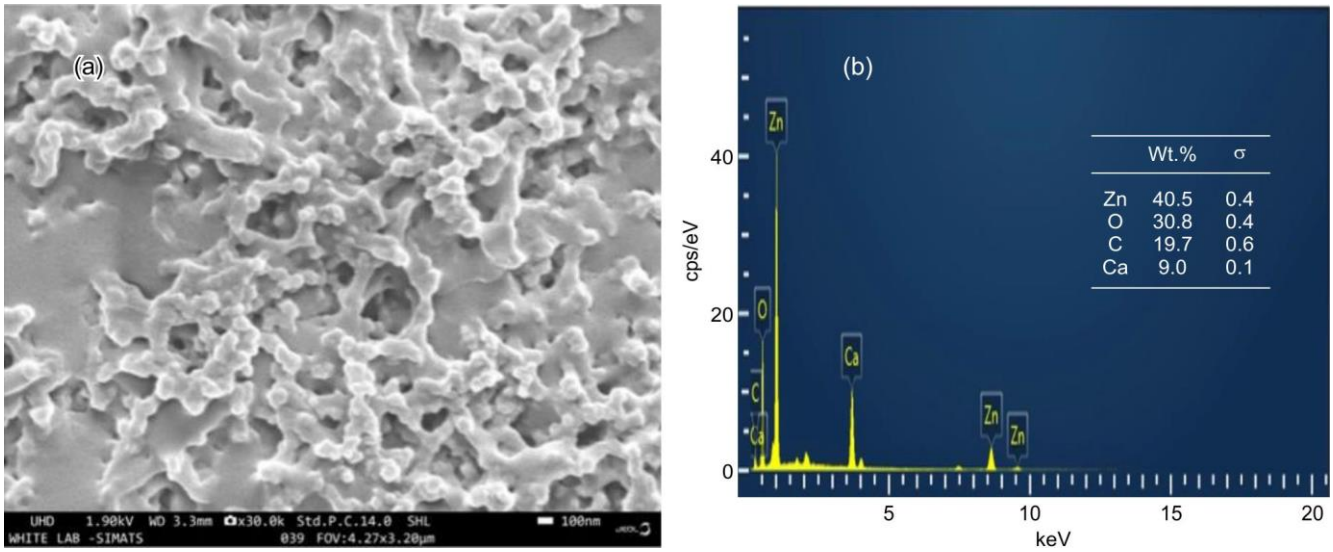

Fig. 4. FE-SEM (a) and EDX (b) spectra of SI-ZnO NPs biosynthesized by *S. isoetifolium*

However, it is well-recognized for its ability to shift from a commensal organism to a pathogenic condition, resulting in various oral diseases such as dental caries, periodontal diseases and oral carcinoma [34]. Its interaction with oral microbiota results in polymicrobial biofilms, potentially elevating virulence. Also, these biofilms serve as a protective barrier, making them more resistant to therapeutic interventions [35]. For instance, Sateriale *et al.* [36] and Mauramo *et al.* [37] reported that bacteria in oral biofilms exhibited anti-biotic tolerance and resistance to the host's immune response. To combat this problem, researchers have focused on developing nanoparticle based implant coatings to ward off infection. Herein, the res*-ults of the biofilm inhibitory assay implied that SI-ZnO NPs significantly ($p < 0.05$) impeded biofilm formation, with inhibition increasing steadily as the concentrations increased to 10 µg/mL (12%), 20 µg/mL (24%), 40 µg/mL (41%), 80 µg/mL (58%), 160 µg/mL (67%) and 320 µg/mL (84%) (Fig. 6).

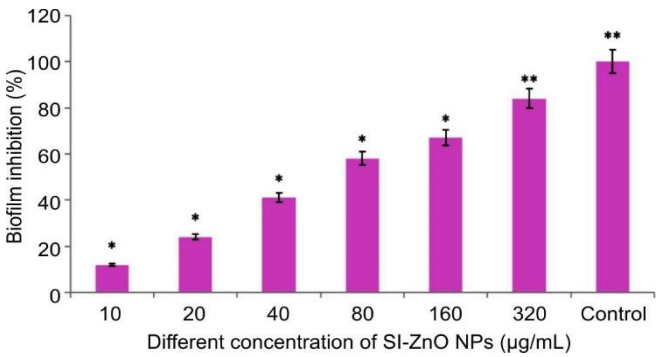

Fig. 6. Biofilm inhibitory activity (%) of SI-ZnONPs biosynthesized by *S. isoetifolium.* The mean ± SD of triplicates indicates a significant percentage of biofilm inhibition of *C. albicans* in different concentrations of SI-ZnO NPs (One-way ANOVA, Dunnett test, *$p < 0.05$)

Confocal Laser Scanning Microscopy (CLSM) analysis revealed a significant reduction in *C. albicans* biofilm formation on the glass substrate following treatment with SI-ZnO NPs at concentrations of 160 and 320 µg/mL (Fig. 7), thereby confirming their potent antibiofilm activity. Previously, Jalal *et al.* [38] revealed that ZnO NPs synthesized through a biogenic method had effectively curtailed biofilm formation by *C. albicans* up to 85% at 250 µg/mL. The potential of ZnO NPs to combat *C. albicans* biofilm has yet to be investigated. However, previous research opined that nanoparticles inhibit *C. albicans* biofilm formation by impeding exopolysaccharide disruption and quorum sensing. As discussed earlier, biofilms formed by *C. albicans* exhibit a natural resistance to standard antifungal treatments, immune responses from the host and various environmental disturbances, presenting a significant challenge in clinical settings [39]. Therefore, incorporating SI-ZnO NPs into implant coatings can significantly inhibit colonization and biofilm formation by *C. albicans* and lower the risk of contact infection. Studies have also demonstrated that coating ZnO on 316L implants significantly improved biocompatibility and osseointegration, pivotal for successful orthopaedic applications [40].

Cytotoxicity activity: The artemia cytotoxicity results indicated that SI-ZnO NPs showed a dose-dependent rise in the mortality of *A. salina*. At the lowest concentration tested (50 µg/mL), no mortality (0%) was observed. However, mortality increased with concentration, reaching 13% at 75 µg/mL, 30% at 100 µg/mL, 47% at 125 µg/mL, and 67% at 150 µg/mL. A marked increase was observed at 175 µg/mL with 83% mortality, culminating in complete mortality (100%) at 200 µg/mL. The calculated LC_{50} value was 62.48 µg/mL (Fig. 8). In concordance with the results of the present study, Bhuvaneshwari *et al.* [41] and Casiano-Muñiz [42] studied the effect of ZnO NPs on *A. salina* and showed LC_{50} values of 71.63 µg/mL and 86.95 µg/mL, respectively. The significant variation in cytotoxicity may be attributed to differences in nanoparticle size. Studies indicate that the mortality rate (%) of *A. salina* changes according to the nanoparticle size. For instance, nanoparticles ranged between 10 and 30 nm show higher mortality than larger nanoparticles (200 nm). Also, a significant mortality (%) variation was observed between nanoparticles of similar sizes [43].

Hemolytic studies: Investigating the hemolytic properties of nanoparticles and bioactive compounds is a benchmark for assessing their toxicity, as it involves spectrophotometric quantification of the lysed RBCs. Accordingly, in present study, the hemolytic activity of SI-ZnO NPs was studied in a dose-dependent manner (Fig. 9). It was observed

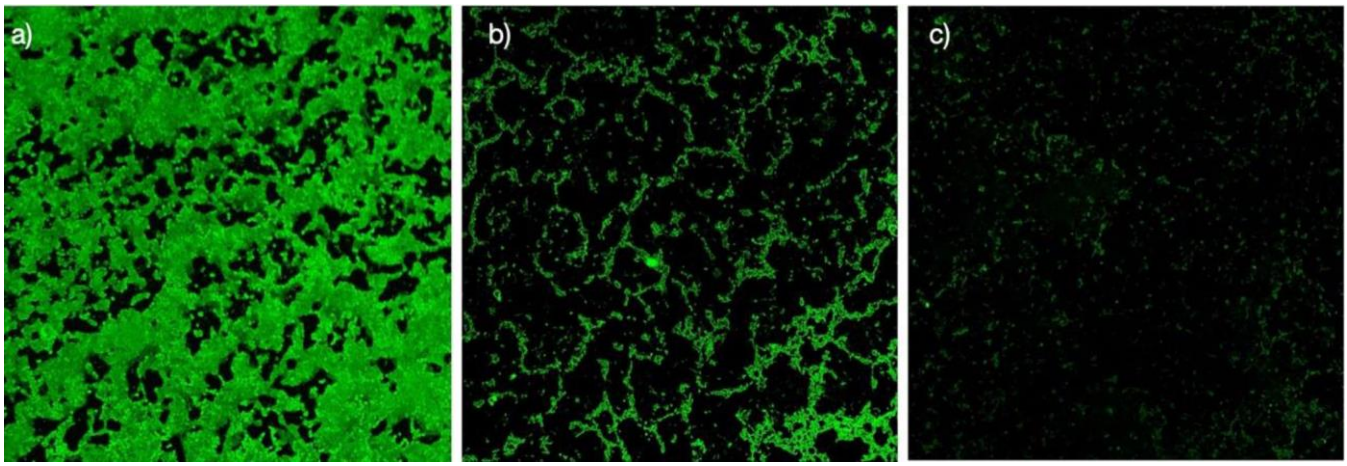

Fig. 7. Antibiofilm activity of SI-ZnO NPs against *C. albicans* [(a) control; (b) 160 µg/mL; (c) 320 µg/mL]

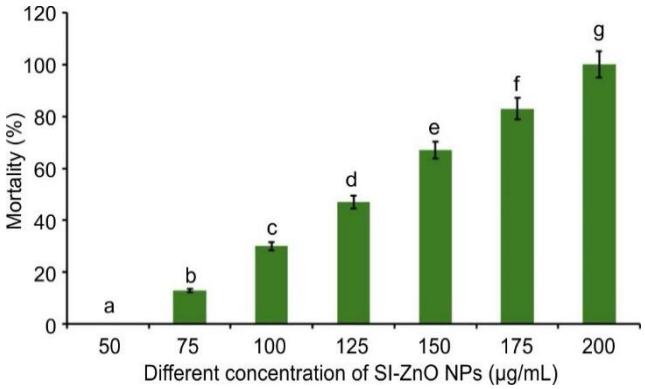

Fig. 8. Artemia cytotoxicity of SI-ZnO NPs. Each set of bars implies different concentrations of SI-ZnO NPs (a-d) with different superscript letters are statistically significant (One-Way ANOVA test; $p < 0.05$, further, the *post hoc* multiple comparisons with SNK test)

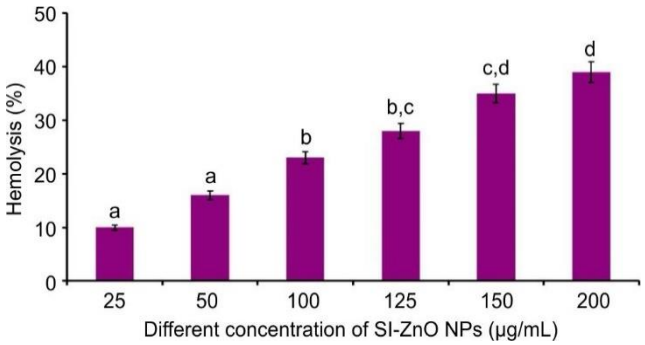

Fig. 6. Hemolytic activity of SI-ZnO NPs. Each set of bars implies different concentrations of SI-ZnO NPs (a-g) with different superscript letters are statistically significant (One-Way ANOVA test; $p < 0.05$, further, the *post hoc* multiple comparisons with SNK test)

that at 25 µg/mL concentration, the percentage of hemolysis was 10%, but further increase in concentrations showed a progressive rise in hemolysis (50 µg/mL - 16%, 100 µg/mL - 23%, 125 µg/mL - 28%, 150 µg/mL - 35%) and reached a maximum of 39% hemolysis at 200 µg/mL. These results indicate that the higher concentration (200 µg/mL) of SI-ZnO NPs showed > 61% viability of RBCs. Preedia Babu *et al.* [44] also investigated the effect of different sizes (< 50 nm, 50-100 nm and > 100 nm) of ZnO NPs on hemolysis and inferred that ZnO NPs smaller than 50 nm exhibited greater hemolytic activity, with only 60% RBCs viability, while large-sized ZnO NPs recorded much lower hemolytic activity with < 80% (50-100 nm) and < 90% (> 100 nm) RBCs viability, respectively. This finding aligns with the current study, which implied that SI-ZnO NPs (67.24 nm) were non/less-toxic. Also, validating the findings of present study, Chen *et al.* [45] reported that smaller nanoparticles exert more toxicity than larger particles, as smaller nanoparticles can easily pass through the RBCs membrane due to their higher surface-to-volume ratio and thereby strongly interact with biomolecules, triggering reactive oxygen species and results in oxidative stress.

Conclusion

In this research, zinc oxide nanoparticles were synthesized using the seagrass *Syringodium isoetifolium*. The change in the colour of the solution from brownish yellow to pale white confirms the synthesis of *S. isoetifolium* mediated ZnO NPs. The biosynthesized SI-ZnO NPs were crystalline, granular and irregularly shaped cubic crystals. *In vitro* antioxidant activity through DPPH radicals suggested that SI-ZnO NPs could efficiently neutralize free radicals, thereby validating their appreciable antioxidant activity. Biofilm inhibitory activity and CLSM visuals manifested that SI-ZnO NPs distorted the structural integrity of the *C. albicans* biofilms and also exerted cytotoxicity against *A. salina* nauplii. Hemolysis assay results underscore the biosafety of the ZnO NPs for further investigation. The promising antioxidant, antibiofilm and cytotoxic properties of SI-ZnO NPs observed in the present study proved it to be a viable solution for therapeutic applications. However, further *in vivo* studies and an understanding of the mechanism of action of SI-ZnO NPs could open new avenues for their utilization in biomedicine.

ACKNOWLEDGEMENTS

The authors gratefully acknowledge Saveetha Dental College and Hospitals, SIMATS, for their support.

CONFLICT OF INTEREST

The authors declare that there is no conflict of interests regarding the publication of this article.

REFERENCES

1. S. Bayda, M. Adeel, T. Tuccinardi, M. Cordani, and F. Rizzolio, *Molecules*, **25**, 112 (2019); https://doi.org/10.3390/molecules25010112
2. M. Sajid, *Curr. Opin. Environ. Sci. Health*, **25**, 100319 (2022); https://doi.org/10.1016/j.coesh.2021.100319
3. X. Ma, Y. Tian, R. Yang, H. Wang, L.W. Allahou, J. Chang, G. Williams, J.C. Knowles and A. Poma, *J. Nanobiotechnol.*, **22**, 715 (2024); https://doi.org/10.1186/s12951-024-02901-x
4. R.A. Banjara, A. Kumar, R.K. Aneshwari, M.L. Satnami and S.K. Sinha, *Environ. Nanotechnol. Monit. Manage.*, **22**, 100988 (2024); https://doi.org/10.1016/j.enmm.2024.100988
5. K.K. Annamalai, B. Selvaraj, K. Subramanian, R. Binsuwaidan and M. Saeed, *Microb. Pathog.*, **193**, 106740 (2024); https://doi.org/10.1016/j.micpath.2024.106740
6. N. Prakashkumar, A. Pugazhendhi, K. Brindhadevi, H.A. Garalleh, M. Garaleh and N. Suganthy, *Environ. Res.*, **220**, 115136 (2023); https://doi.org/10.1016/j.envres.2022.115136
7. M.A. Peres, L.M. Macpherson, R.J. Weyant, B. Daly, R. Venturelli, M.R. Mathur, S. Listl, R.K. Celeste, C.C. Guarnizo-Herreño, C. Kearns, H. Benzian, P. Allison and R.G. Watt, *Lancet*, **394**, 249 (2019); https://doi.org/10.1016/S0140-6736(19)31146-8
8. X. Niu, X. Rong and H. Sun, *J. Dent. Sci.*, **9**, 1 (2023); https://doi.org/10.1016/j.jds.2023.09.030
9. M.A. Al-Shahrani, *Ann. Med. Health Sci. Res.*, **9**, 655 (2019).
10. G. Eidt, E.D. Waltermann, J.B. Hilgert and A. Arthur, *Arch. Oral Biol.*, **119**, 104876 (2020); https://doi.org/10.1016/j.archoralbio.2020.104876
11. X. Huang, Q. Dong, Q. Zhou, S. Fang, Y. Xu, H. Long, J. Chen, X. Li, H. Qin, D. Mu and X. Cai, *Front. Microbiol.*, **16**, 1531543 (2025); https://doi.org/10.3389/fmicb.2025.1531543
12. M. Fan, Y. Liu, Y.Q. Liu, R.X. Lv, W. Sun, W.J. Ding, Y.X. Cai, W.W. Li, X. Liu and W. Qu, *Int. J. Antimicrob. Agents*, **60**, 106673 (2022); https://doi.org/10.1016/j.ijantimicag.2022.106673
13. M.M. Mamun, A.J. Sorinolu, M. Munir and E.P. Vejerano, *Front Chem.*, **9**, 687660 (2021); https://doi.org/10.3389/fchem.2021.687660
14. J.A. Edson and Y.J. Kwon, *Nano Converg.*, **3**, 26 (2016); https://doi.org/10.1186/s40580-016-0085-7
15. A.L. Francis, S.K.R. Namasivayam and K. Samrat, *Microb. Pathog.*, **196**, 106957 (2024); https://doi.org/10.1016/j.micpath.2024.106957

16. S. Barathi, S. Ramalingam, G. Krishnasamy and J. Lee, *Pharmaceutics*, **16**, 923 (2024); https://doi.org/10.3390/pharmaceutics16070923
17. C. Ragavendran, C. Kamaraj, K. Jothimani, A. Priyadharsan, D. Anand Kumar, D. Natarajan and G. Malafaia, *SM&T*, **36**, e00597 (2023); https://doi.org/10.1016/j.susmat.2023.e00597
18. J.P. Jaison, B. Balasubramanian, J. Gangwar, M. Pappuswamy, A. Meyyazhagan, H. Kamyab, K.A. Paari, W.-C. Liu, M.M. Taheri and K.S. Joseph, *Bioprocess Biosyst. Eng.*, **47**, 1605 (2024); https://doi.org/10.1007/s00449-024-03036-x
19. R. Coles, F. Short, M. Fortes and J. Kuo, *Pac. Conserv. Biol.*, **20**, 8 (2014); https://doi.org/10.1071/PC140008
20. H.M. Ameen, A. Jayadev, G. Prasad and D.I. Nair, *Molecules*, **29**, 4596 (2024); https://doi.org/10.3390/molecules29194596
21. N.K. Ahila, V.S. Ramkumar, S. Prakash, B. Manikandan, J. Ravindran, P.K. Dhanalakshmi and E. Kannapiran, *Biomed. Pharmacother.*, **84**, 60 (2016); https://doi.org/10.1016/j.biopha.2016.09.004
22. P.D. Thinh, A.B. Rasin, A.S. Silchenko, V.T. Trung, M.I. Kusaykin, C.T.T. Hang, E.S. Menchinskaya, E.A. Pislyagin and S.P. Ermakova, *Int. J. Biol. Macromol.*, **242**, 124714 (2023); https://doi.org/10.1016/j.ijbiomac.2023.124714
23. M. Narayanan, S. Srinivasan, C. Gnanasekaran, G. Ramachandran, C.K. Chelliah, G. Rajivgandhi, M. Maruthupandy, F. Quero, W.J. Li, G. Hayder, J.M. Khaled, A. Arunachalam and N. Manoharan, *Microb. Pathog.*, **189**, 106595 (2024); https://doi.org/10.1016/j.micpath.2024.106595
24. V. Sundar, B. Balasubramanian, M. Sivakumar, S. Chinnaraj, V. Palani, V. Maluventhen, H. Kamyab, S. Chelliapan, M. Arumugam and D. Patricia Zuleta Mediavilla, *Inorg. Chem. Commun.*, **161**, 112125 (2024); https://doi.org/10.1016/j.inoche.2024.112125
25. S. Prakash, R. Ramasubburayan, V.S. Ramkumar, E. Kannapiran, A. Palavesam and G. Immanuel, *Biomed. Pharmacother.*, **83**, 648 (2016); https://doi.org/10.1016/j.biopha.2016.07.019
26. J. Soni, D. Revathi, G. Dhanraj and R. Ramasubburayan, *Microb. Pathog.*, **193**, 106758 (2024); https://doi.org/10.1016/j.micpath.2024.106758
27. H. Hameed, A. Waheed, M.S. Sharif, M. Saleem, A. Afreen, M. Tariq, A. Kamal, W.A. Al-Onazi, D.A. Al Farraj, S. Ahmad and R.M. Mahmoud, *Micromachines*, **14**, 928 (2023); https://doi.org/10.3390/mi14050928
28. S. Rajeswaran, S. Somasundaram Thirugnanasambandan, S. Rengasamy Subramaniyan, S. Kandasamy and R. Vilwanathan, *Appl. Phys., A Mater. Sci. Process.*, **125**, 105 (2019); https://doi.org/10.1007/s00339-019-2404-4
29. A.T. Mansour, A.E. Alprol, M. Khedawy, K.M. Abualnaja, T.A. Shalaby, G. Rayan, K.M.A. Ramadan and M. Ashour, *Materials*, **15**, 5169 (2022); https://doi.org/10.3390/ma15155169
30. P. More, V. Inamdar, S. Suresh, S. Dindorkar, S. Peddakolmi, K. Jain, N. Khona, S. Khatoon and S. Patange, *J. Mater. Sci. Mater. Electron.*, **32**, 20725 (2021); https://doi.org/10.1007/s10854-021-06585-z
31. D. Rehana, D. Mahendiran, R.S. Kumar and A.K. Rahiman, *Bioprocess Biosyst. Eng.*, **40**, 943 (2017); https://doi.org/10.1007/s00449-017-1758-2
32. S. Vijayakumar, S. Mahadevan, P. Arulmozhi, S. Sriram and P.K. Praseetha, *Mater. Sci. Semicond. Process.*, **82**, 39 (2018); https://doi.org/10.1016/j.mssp.2018.03.017
33. C. Chinnasamy, P. Tamilselvam, B. Karthick, B. Sidharth and M. Senthilnathan, *Mater. Today Proc.*, **5**, 6728 (2018); https://doi.org/10.1016/j.matpr.2017.11.331
34. K.K.R. Ealla, N. Kumari, S. Chintalapani, S. Uppu, V. Sahu, V.P. Veeraraghavan, P. Ramani and S.R. Govindool, *Arch. Microbiol.*, **206**, 127 (2024); https://doi.org/10.1007/s00203-024-03856-1
35. M. RapalaKozik, M. Surowiec, M. Juszczak, E. Wronowska, K. Kulig, A. Bednarek, M. Gonzalez-Gonzalez, J. Karkowska-Kuleta, D. Satala M. Zawrotniak and A. Kozik, *Yeast*, **40**, 303 (2023); https://doi.org/10.1002/yea.3855
36. D. Sateriale, R. Imperatore, R. Colicchio, C. Pagliuca, E. Varricchio, M.G. Volpe, P. Salvatore, M. Paolucci and C. Pagliarulo, *Front. Microbiol.*, **11**, 592265 (2020); https://doi.org/10.3389/fmicb.2020.592265
37. M. Mauramo, N. Tonoz, J. Halter, B. Joseph and T. Waltimo, *Support. Care Cancer*, **32**, 185 (2024); https://doi.org/10.1007/s00520-024-08396-4
38. M. Jalal, M.A. Ansari, S.G. Ali, H.M. Khan and S. Rehman, *Artif. Cells Nanomed. Biotechnol.*, **46(sup1)**, 912 (2018); https://doi.org/10.1080/21691401.2018.1439837
39. M. Gulati and C.J. Nobile, *Microbes Infect.*, **18**, 310 (2016); https://doi.org/10.1016/j.micinf.2016.01.002
40. M. Mehdizade, A.R. Eivani, O. Esmaielzadeh and P. Rostamian, *J. Mater. Res. Technol.*, **28**, 935 (2024); https://doi.org/10.1016/j.jmrt.2023.12.027
41. M. Bhuvaneshwari, B. Sagar, S. Doshi, N. Chandrasekaran and A. Mukherjee, *Environ. Sci. Pollut. Res. Int.*, **24**, 5633 (2017); https://doi.org/10.1007/s11356-016-8328-z
42. I.M. Casiano-Muñiz, M.I. Ortiz-Román, G. Lorenzana-Vázquez and F.R. Román-Velázquez, *Nanomaterials*, **14**, 255 (2024); https://doi.org/10.3390/nano14030255
43. M. Ates, J. Daniels, Z. Arslan, I.O. Farah and H.F. Rivera, *Environ. Sci. Process. Impacts*, **15**, 225 (2013); https://doi.org/10.1039/C2EM30540B
44. E. Preedia Babu, A. Subastri, A. Suyavaran, K. Premkumar, V. Sujatha, B. Aristatile, G.M. Alshammari, V. Dharuman and C. Thirunavukkarasu, *Sci. Rep.*, **7**, 4203 (2017); https://doi.org/10.1038/s41598-017-04440-y
45. L.Q. Chen, L. Fang, F. Ling, C.Z. Ding, B. Kang and C.Z. Huang, *Chem. Res. Toxicol.*, **28**, 501 (2015); https://doi.org/10.1021/tx500479m